Water Desalination Using Nanoporous Single-Layer Graphene with Tunable Pore Size

Sumedh P. Surwade,[1] Sergei N. Smirnov,[2] Ivan V. Vlassiouk,[3*] Raymond R. Unocic,[4] Sheng Dai,[1,5]* Shannon M. Mahurin[1]*

[1]Chemical Sciences Division, Oak Ridge National Laboratory, Oak Ridge, TN 37831
[2] Dept. of Chemistry and Biochemistry, New Mexico State University, Las Cruces, NM, 88003
[3]Energy and Transportation Science, Oak Ridge National Laboratory, Oak Ridge, Tennessee 37831, United States
[4]Center for Nanophase Materials Sciences, Oak Ridge National Laboratory, Oak Ridge, TN 37831
[5]Dept. of Chemistry, University of Tennessee, Knoxville, TN 37996

*Correspondence to: mahurinsm@ornl.gov, vlassioukiv@ornl.gov, dais@ornl.gov

Abstract
Graphene has great potential to serve as a separation membrane due to its unique properties such as chemical and mechanical stability, flexibility and most importantly its one-atom thickness. In this study, we demonstrate first experimental evidence of the use of single-layer porous graphene as a desalination membrane. Nanometer-sized pores are introduced into single layer graphene using a convenient oxygen plasma etching process that permits tuning of the pore size. The resulting porous graphene membrane exhibited high rejection of salt ions and rapid water transport, thus functioning as an efficient water desalination membrane. Salt rejection selectivity of nearly 100% and exceptionally high water fluxes exceeding 10^5 g m^{-2} s^{-1} at 40 °C were measured using saturated water vapor as a driving force.

Although water covers approximately 75% of the surface of the earth, scarcity of fresh water is a serious global challenge that is predicted to worsen in the future as demand continues rising due to population growth, increased industrialization and greater energy needs.[1,2] Because seawater represents such a vast supply, desalination has become an important and promising approach to meet this ever-increasing demand for fresh water. Membrane-based separation of water using techniques such as reverse osmosis offers the highest energy efficiency while maintaining the capability for use at industrial scales. There has been significant interest in graphene, a two-dimensional allotrope of carbon, as the ultimate membrane material because it is extremely thin at only one carbon atom, is extremely strong, and can be chemically modified.

A number of theoretical studies have predicted that graphene with sub-nanometer pores can act as a highly selective and permeable filtration membrane with greater efficiency than current state-of-the-art polymer-based filtration membranes.[3-11] Following these theoretical predictions, a few experimental studies have begun to explore the use of both graphene and graphene oxide for membrane separation with promising results. For example, Koenig et al. demonstrated selective gas transport through porous single and bilayer graphene obtained using mechanical exfoliation and oxidative etching.[12] Selective gas transport for H_2/CO_2, H_2/N_2 and CO_2/N_2 has also been reported using graphene oxide membranes.[13,14] In addition, Garaj and co-workers created nanoporous graphene that functioned as trans-electrode membranes and demonstrated DNA translocation through single nanopores[15] while Shan et al. similarly used it for translocation of proteins.[16] Interestingly, O'Hern et al. recently reported both selective ion and molecular transport through single layer graphene membranes with subnanometer pores.[17,18] For the ion selective graphene membrane, the pore size was tuned using ion bombardment and oxidative etching to permit salt transport while preventing transport of organic dye molecules.

Here we experimentally examine the transport of ions and water across a suspended, single-layer graphene membrane with nanometer-sized pores that were generated by oxygen plasma etching in order to validate the effectiveness of graphene-based desalination of water. These membranes exhibit both high salt rejection and exceptionally rapid water transport properties. Using aberration-corrected scanning transmission electron microscopy (STEM) imaging, we correlate the porosity of the graphene membrane with transport properties and determine the optimum pore size for effective desalination. The mechanism of water transport is explored suggesting that graphene may be suitable both for membrane distillation and reverse osmosis.

Results

Single layer graphene was synthesized using a previously-reported method of ambient pressure chemical vapor deposition (CVD) on a copper foil catalyst.[19] The graphene was subsequently transferred onto a silicon nitride (SiN) microchip device that contains a single 5 μm hole (prepared by a standard clean room techniques)[20] using a standard polymer transfer method with poly(methyl methacrylate) (PMMA). Scanning electron microscopy (SEM) imaging confirmed that the graphene layer suspended over the hole was intact with no visible ruptures or tears (see Fig. 1A). This approach was quite effective with more than 70% of transfer attempts yielding functional devices after SEM inspection. The quality of the suspended graphene was then evaluated using Raman spectroscopy. It should be noted that the laser spot of the Raman instrument was approximately 3 μm which is smaller than the hole size in the SiN microchip thereby allowing us to measure the spectrum of only the suspended portion of the graphene. From the Raman spectra in Fig. 1B, pristine, suspended graphene exhibited a strong G peak (~1580 cm^{-1}) with no discernable defect peak, D, at 1350 cm^{-1}. The absence of a D peak

suggests high quality graphene with a negligible number of defects introduced during the synthesis and transfer steps. Moreover, the 2D peak (~2700 cm^{-1}) is ~ 3 times stronger than the G peak with a line width <30 cm^{-1} (Lorentzian lineshape) again indicating that the graphene is single layer.[21] The synthesis conditions were chosen to generate graphene domains in excess of 50 μm [22] making the incidence of grain boundaries directly over the 5μm holes highly unlikely, in agreement with the Raman measurements.

Nanopores were then introduced on the suspended graphene by exposure to oxygen plasma with a power of ~20 W for different times. As indicated by the Raman spectra in Fig. 1B, the intensity of the D peak increased with increasing exposure time. Even after a short irradiation time of only 0.5 s, the D peak intensity rose to 1/3 of that for the G peak (I_D/I_G ~ 0.333). After a longer exposure of 6 s, the 2D peak completely disappeared while the D and G peaks broadened to resemble those of a disordered carbon material indicating significant defect formation. The ratio of I_D/I_G has been extensively used as a measure of the integrity of graphene and we will use it here as a convenient measure of defects as well.[23,24] However, it is important to note that Raman analysis does not provide comprehensive information about the various types of defects that may be present. As an example, we explored alternative methods of defect formation such as bombardment of electrons of different energies (250 V-20 kV) as well as gallium ions of 30 kV (supplemental materials) but observed negligible species transport through these membranes in contrast to the oxygen plasma treatment, despite similar variations in the Raman spectra.

We measured the water transport properties of various plasma-etched graphene membranes using deionized (DI) water and 6mM KCl. The SiN microchip device (5 μm hole) with the suspended graphene membrane was sealed on top of a container partially filled with DI

water using epoxy. By inverting the container, the water came in direct contact with the graphene membrane and, because of the epoxy seal, the only transport path available was through the porous graphene (Fig. 2A). The container was then placed inside an oven maintained at 40 °C and the water transport was determined by measuring the mass of the water-filled container at regular time intervals and noting the mass decrease. The amount of water loss through pristine graphene, plasma-etched graphene and a control (open 5 μm hole with no graphene) after 24 h are shown in Fig. 2B. As expected, the control exhibited the largest mass loss since there was no graphene to inhibit water transport. The pristine, non-etched graphene with $I_D/I_G = 0$ showed no water loss after 24 h indicating an intact membrane with no holes or tears in agreement with prior SEM and Raman results. This also agrees with previous reports demonstrating the impermeability of pristine graphene sheets.[25] In contrast, the porous, plasma-etched graphene samples did show water loss and the rate of water transport was dependent on the plasma etching time. Even for the shortest exposure times with low defect density (I_D/I_G ~0.5), the porous graphene membranes showed an unexpectedly high water loss rate that was only 3 times less than the control with an open 5 μm diameter hole. As the defect density increased, the water transport rate increased reaching 60% of the control value for graphene with $I_D/I_G \sim 2$.

After verifying that water could flow through the porous graphene membrane, the next step was to measure the ion transport behavior. To that end, the same membranes used for water transport were analyzed for ion transport using 1 M KCl (or NaCl and LiCl) solutions in a custom electrochemical cell (see supplemental materials).[26] As shown in Fig. 2B, the ionic current through the porous graphene membrane with a low defect density ($I_D/I_G \leq 0.5$) was almost non-existent (i.e., no transport of ions) suggesting extremely small pores while the ionic

current in the graphene membrane with high defect density, $I_D/I_G > 1$, was much greater indicating the presence of larger pores. Not surprisingly, the control sample (C2) with the open 5 μm hole had the highest ionic current, and the highest rate of water transport. From these results, we note that the porous graphene membrane with low defect density, $I_D/I_G \leq 0.5$, showed both extremely low ionic current and measurable water transport, *i.e.*, it successfully functioned as a desalination membrane demonstrating effective salt rejection. The selectivity values were calculated as the ratio of water flux to salt transport normalized to the fluxes through pores without a graphene membrane (Eq.1).

$$S = \frac{J_{H_2O}}{J_{\max}} \Big/ \frac{I_{salt}}{I_{\max}} \qquad (1)$$

where J_{H2O} and I_{salt} are the water flux and the ionic current through graphene membrane, correspondingly, while J_{max} and I_{max} are the water flux and the ionic current though a 5 μm hole in SiN membrane without graphene (C2 sample). For such a definition of selectivity, S = 1 for a fully non-selective membrane while S > 1 for a membrane that is selective toward water molecules and rejects dissolved ions.

In an alternative experiment, a salt solution of water (conductivity of 950 μS/cm) (Table 1) was used to simultaneously measure both water transport and ion transport through the graphene membrane. In this measurement, the permeate water was collected using a second container mounted beneath the membrane and sealed from the atmosphere to prevent evaporation of the permeate water (see the supplemental materials). The water transport rate for the salt solution was comparable to the pure DI water measurement previously described. However, the conductivity of the permeate solution was < 11 μS/cm, or almost three orders of magnitude

lower than the feed salt solution, confirming that the porous graphene functioned as a desalination membrane.

Thus both experiments confirmed a high selectivity in water transport through oxygen plasma-treated single layer graphene membranes. As Fig. 2B demonstrates, the salt rejection for the low defect density membranes was exceptionally high. The selectivity of the porous graphene membrane with $I_D/I_G \leq 0.5$ was almost $S \sim 10^5$, which corresponds to nearly 100% salt rejection. It dropped precipitously to $S \sim 10$ for $I_D/I_G \sim 2$, which indicates that extended plasma exposure not only increases the number of defects in the graphene but also enlarges the pores as well.

We analyzed the porous membranes using aberration-corrected STEM (see Fig. 3). Based on the medium angle annular dark field (MAADF) STEM images, the pore sizes are in the range of 0.5 nm to 1 nm, which is consistent with the anticipated optimal pore size for rejecting small ions while still permitting water transport. We did not observe large pores, which are probably more difficult to eliminate in samples of larger area. Raman measurements for the sample in Fig. 3 reveal that the I_D/I_G ratio is approximately one, which suggests that the pore density is on the order of 1 pore/100 nm^2 in agreement with evaluation of the STEM images (see Supplemental).

Theoretical studies of water transport through graphene membranes have predicted that hydrogenated pores less than 2.3 nm in diameter and hydroxylated pores less than 1.6 nm on the graphene surface can retain salt ions while allowing water molecules to pass through at a fairly high rate.[4] The estimated theoretical salt rejection was close to 100% for the pores of these sizes but decreased in slightly larger pores. At the same time, reported experimental findings have shown very promising results but highlight the lack of a convenient method to produce small diameter nanopores in graphene. For example, irradiation by either electrons or atomic ions generate relatively small pores that are not large enough or simply produce defects that are

mostly lattice rearrangements or rare knock-off of individual carbon atoms. Treatment in high temperature oxygen,[27,28] hydrogen,[29] or oxidizing reagents[17] can produce nanopores which fall into the desired range, however, the size distribution of such pores is difficult to control. As shown in a recent paper from O'Hern et al.,[17] even for pores with a diameter of 0.40 ± 0.24 nm, cleverly obtained by permanganate etching of defects previously introduced by Ga ion irradiation, the ionic flux was not well rejected because the process also resulted in a significant fraction of larger pores that permitted passage not only of small ions (K^+ and Cl^-) but molecular ions as well.

In contrast, our graphene membranes plasma-etched for short exposure times exhibited an extremely high salt rejection rate which could be due to a number of reasons. First, though plasma treatment has been considered in the past as a possible method to generate pores in graphene, it has typically been used for graphene lying on a substrate. In the suspended graphene used for our membranes, the rate of defect production and the morphology of the pores likely vary compared to supported graphene. Second, it has been well illustrated that structural defects in graphene such as grain boundaries are the most vulnerable points for chemical alteration.[30,31] Our membranes, however, are composed of monocrystalline single layer graphene that is less prone to chemical modification - the active size of the graphene membrane suspended over the hole is significantly smaller than the domain size of the synthesized graphene. [22] Finally, our plasma-etching treatment combines a similar defect production capability exhibited by high energy ion bombardment with a time-tuned oxidative atmosphere, all with a minimum number of steps, each of which increases the potential for mechanical disruption and tear formation.[17] We have observed some of the advantages of oxygen plasma treatment of

suspended (multilayer) graphene in a previous study of surface treatment effects of graphene in designing nanopores for protein translocation.[16]

One intriguing observation was the exceptionally high rate of water transport through the porous graphene, which was much higher than previously reported,[3] despite the nearly 100% salt rejection rate. In the experiment, the graphene was in direct contact with the water and the total driving pressure across the graphene membrane, which was provided by gravity and the vapor pressure of water at 40 °C, was estimated to be approximately 8 kPa. For the control sample with no graphene over the 5 μm open hole, the water flow rate was measured to be approximately 0.30 g h^{-1} (or 4.2×10^{6} g m^{-2} s^{-1}), which is close to that estimated from the Hagen−Poiseuille expression with entrance/exit loss:

$$Q = \frac{\Delta P}{\mu}\frac{R^3}{C + \frac{8L}{\pi R}} \qquad (2)$$

where C~1.5 is the loss coefficient, R and L are the SiN pore radius and length, ΔP is the driving pressure and μ is the water dynamic viscosity.[32] For the porous graphene membranes with I_D/I_G~0.5, the water flux was ~20% of the flux through the open 5 μm hole. Careful inspection of the samples presented in Figs. 1 and 2 eliminated any possibility of tears in the graphene membrane and the absence of salt transport confirmed that. These results imply that there were no large pores but rather water transport through the graphene nanopores was somehow enhanced.

Nair et al.[3] recently demonstrated that graphene-based membranes made of multiple layers of graphene oxide are specifically permeable to water, while impenetrable by other molecules including helium. The rate of water vapor permeation through the membrane was almost identical to that of an uncovered opening. The authors explained this by a unique low-

friction flow of water monolayers through two-dimensional capillaries formed by closely spaced graphene sheets. We believe that a similar effect of water movement near the graphene surface is involved here but the details require further investigation. Regardless, the effective flux achieved through our porous graphene membranes was 5 orders of magnitude greater than that reported by Nair et al.[3]

In conclusion, we have shown the potential utility of nanoporous graphene as a selective membrane which can be used for water desalination. We have shown that oxygen plasma can be used as a very convenient method for the fabrication of tailored nanopores of desired dimension (and probably chemical properties) in suspended single layer graphene with a precision not attained by other approaches. The resulting nanopores showed tremendous water molecule selectivity over dissolved ions (K^+, Na^+, Li^+, Cl^-). The selectivity exceeded five orders of magnitude for low porosities but precipitously decreased at higher porosities most likely due to the enlargement of nanopores. Based on the estimated density of nanopores by Raman and STEM, ~1/100 nm^2, the estimated water flux through a single nanopore can reach tremendously high values of 3-4 molecules per ps, which exceeds the flux through aquaporin channels by three orders of magnitude and approximately by an order of magnitude greater than estimated from MD simulations for similar size pores. [3-11]

Methods

Single-layer graphene was synthesized by an ambient pressure chemical vapor deposition (CVD) process using a copper foil catalyst in methane and hydrogen atmosphere. The partial pressures of the individual gases were set using flow controllers with stock gases. Prior to synthesis, the copper foil catalyst was annealed in a hydrogen/Ar mixture at the growth temperature for approximately 30 min. The graphene was transferred to a SiN wafer with a 5 μm hole using poly (methyl methacrylate) (PMMA). The PMMA was coated onto the copper with graphene and the

copper was removed using $FeCl_3$. After rinsing, the PMMA/graphene was placed on the SiN wafer and the PMMA was removed using acetone followed by thermal annealing. The pristine graphene was characterized using both Raman spectroscopy and electron microscopy to ensure there were no large defects. Pores were introduced into the graphene using an oxygen plasma etcher (Diener) at 20 W. Ion transport measurements were made using a 300nm thick SiN membrane with graphene covering a 5μm diameter hole drilled by a focused ion beam mounted in a custom electrochemical cell with two Ag/AgCl wire electrodes on both sides of the membrane. The ionic current was measured by Keithley 6487 picoammeter interfaced by Matlab. Water transport measurements were performed by attaching the SiN microchip device onto the lid of container with a hole punched in it using epoxy. After allowing the epoxy to cure, the lid was placed on the container partially filled with DI water (or KCl solution) and sealed. For pure DI water transport measurements, the container was then inverted so the water was in contact with the graphene and the entire assembly was placed in an oven maintained at 40 °C. The mass of the container was then measured periodically to determine the mass loss and water transport through the membrane.

1 Shannon, M. A. *et al.* Science and technology for water purification in the coming decades. *Nature* **452**, 301-310 (2008).

2 Elimelech, M. & Phillip, W. A. The future of seawater desalination: Energy, technology, and the environment. *Science* **333**, 712-717 (2011).

3 Nair, R. R., Wu, H. A., Jayaram, P. N., Grigorieva, I. V. & Geim, A. K. Unimpeded permeation of water through helium-leak-tight graphene-based membranes. *Science* **335**, 442-444 (2012).

4 Cohen-Tanugi, D. & Grossman, J. C. Water desalination across nanoporous graphene. *Nano Lett.* **12**, 3602-3608 (2012).

5 Jiang, D.E., Cooper, V. R. & Dai, S. Porous graphene as the ultimate membrane for gas separation. *Nano Lett.* **9**, 4019-4024 (2009).

6 Konatham, D., Yu, J., Ho, T. A. & Striolo, A. Simulation insights for graphene-based water desalination membranes. *Langmuir* **29**, 11884-11897 (2013).

7 Suk, M. E. & Aluru, N. R. Water transport through ultrathin graphene. *J. Phys. Chem. Lett.* **1**, 1590-1594 (2010).
8 Du, H. *et al.* Separation of hydrogen and nitrogen gases with porous graphene membrane. *J. Phys. Chem. C* **115**, 23261-23266 (2011).
9 Sint, K., Wang, B. & Kral, P. Selective ion passage through functionalized graphene nanopores. *J. Am. Chem. Soc.* **130**, 16448-16449 (2008).
10 Sun, C. *et al.* Mechanisms of molecular permeation through nanoporous graphene membranes. *Langmuir* **30**, 675-682 (2014).
11 Wang, E. N. & Karnik, R. Water desalination graphene cleans up water. *Nature Nanotechnol.* **7**, 552-554 (2012).
12 Koenig, S. P., Wang, L., Pellegrino, J. & Bunch, J. S. Selective molecular sieving through porous graphene. *Nat. Nanotechnol.* **7**, 728-732 (2012).
13 Kim, H. W. *et al.* Selective gas transport through few-layered graphene and graphene oxide membranes. *Science* **342**, 91-95 (2013).
14 Li, H. *et al.* Ultrathin, molecular-sieving graphene oxide membranes for selective hydrogen separation. *Science* **342**, 95-98 (2013).
15 Garaj, S. *et al.* Graphene as a subnanometre trans-electrode membrane. *Nature* **467**, 190-193 (2010).
16 Shan, Y. P. *et al.* Surface modification of graphene nanopores for protein translocation. *Nanotechnology* **24**, 495102 (2013).
17 O'Hern, S. C. *et al.* Selective ionic transport through tunable subnanometer pores in single-layer graphene membranes. *Nano. Lett.* **14**, 1234-1241 (2014).
18 O'Hern, S. C. *et al.* Selective molecular transport through intrinsic defects in a single layer of cvd graphene. *Acs Nano* **6**, 10130-10138 (2012).
19 Vlassiouk, I. *et al.* Large scale atmospheric pressure chemical vapor deposition of graphene. *Carbon* **54**, 58-67 (2013).
20 Vlassiouk, I., Apel, P. Y., Dmitriev, S. N., Healy, K. & Siwy, Z. S. Versatile ultrathin nanoporous silicon nitride membranes. *Proc. Natl. Acad. Sci.* **106**, 21039-21044 (2009).
21 Malard, L. M., Pimenta, M. A., Dresselhaus, G. & Dresselhaus, M. S. Raman spectroscopy in graphene. *Phys. Rep.* **473**, 51-87 (2009).
22 Vlassiouk, I. *et al.* Graphene nucleation density on copper: Fundamental role of background pressure. *J. Phys. Chem. C* **117**, 18919-18926 (2013).
23 Dresselhaus, M. S., Jorio, A., Hofmann, M., Dresselhaus, G. & Saito, R. Perspectives on carbon nanotubes and graphene raman spectroscopy. *Nano Lett.* **10**, 751-758 (2010).
24 Lucchese, M. M. *et al.* Quantifying ion-induced defects and raman relaxation length in graphene. *Carbon* **48**, 1592-1597 (2010).
25 Bunch, J. S. *et al.* Impermeable atomic membranes from graphene sheets. *Nano Lett.* **8**, 2458-2462 (2008).
26 Smirnov, S. N., Vlassiouk, I. V. & Lavrik, N. V. Voltage-gated hydrophobic nanopores. *ACS Nano* **5**, 7453-7461 (2011).
27 Surwade, S. P., Li, Z. T. & Liu, H. T. Thermal oxidation and unwrinkling of chemical vapor deposition-grown graphene. *J. Phys. Chem. C* **116**, 20600-20606 (2012).
28 Liu, L. *et al.* Graphene oxidation: Thickness-dependent etching and strong chemical doping. *Nano. Lett.* **8**, 1965-1970 (2008).
29 Diankov, G., Neumann, M. & Goldhaber-Gordon, D. Extreme mono layer-selectivity of hydrogen-plasma reactions with graphene. *ACS Nano* **7**, 1324-1332 (2013).

30 Banhart, F., Kotakoski, J. & Krasheninnikov, A. V. Structural defects in graphene. *ACS Nano* **5**, 26-41 (2011).
31 Wang, B., Puzyrev, Y. & Pantelides, S. T. Strain enhanced defect reactivity at grain boundaries in polycrystalline graphene. *Carbon* **49**, 3983-3988 (2011).
32 Weissberg, H. L. End correction for slow viscous flow through long tubes. *Phys. Fluids* **5**, 1033-1036 (1962).

Supplementary Information is linked to the online version of the paper at www.nature.com/nature.

Acknowledgments
Research was sponsored by the Laboratory Directed Research and Development Program of Oak Ridge National Laboratory, managed by UT-Battelle, LLC, for the U. S. Department of Energy. A portion of this research was conducted at the Center for Nanophase Materials Sciences, which is sponsored at Oak Ridge National Laboratory by the Scientific User Facilities Division, U.S. Department of Energy.

Author Contributions S.P.S. and I.V.V.performed graphene synthesis and characterization measurements (ion and water transport measurements). R.R.C. performed the aberration-corrected STEM microscopy. S.M.M, I.V.V and S.D. conceived the idea and designed the experiments. I.V.V., S.M.M. S.P.S., S.N.S. and S.D. analyzed the data and interpreted the results. All authors contributed to the writing of the manuscript.

Author Information Reprints and permission information is available at www.nature.com/reprints. The authors declare no competing financial interests. Correspondence and requests for materials should be addressed to S.M.M (mahurinsm@ornl.gov) and I.V.V. (vlassioukiv@ornl.gov).

Figure Legends:

Figure 1. (A) Schematic and the SEM image of single layer graphene suspended on a 5 μm diameter hole. For nanoporous graphene fabrication, several approaches have been utilized: bombardment by ions, by electrons and via O_2 plasma treatment. (B) Raman spectra (514 nm excitation) of suspended graphene after different exposure times to the oxygen plasma.

Figure 2. (A) Porous graphene membrane assembly for water flux measurements. Graphene membrane on silicon chip with 5μm hole in 300nm thick SiN membrane is sealed on the glass vial filled with DI water. Vial is turned upside down and placed in an oven with 40 °C. Water loss is measured by monitoring the vial's mass. **(B)** Water loss after 24 h and ionic conductivity through the same porous graphene membranes etched at various exposure times. C1 and C2 are controls with large tears or completely broken graphene membranes. **(C)** Water/Salt selectivity as a function of I_D/I_G ratio showing exceptionally high selectivity for short etching time. The selectivity was calculated as a ratio of water flux to ionic conductivity from (B) normalized to water flux and conductivity of pore in SiN without graphene. **(D)** Examples of I-V curves measured in 1M KCl solution across porous graphene membrane for different plasma exposure time. **(E)** Sketch of experimental setup for I-V measurements. Two Ag/AgCl wires were used as electrodes.

Figure 3. (A, B) Aberration-corrected STEM images of graphene after 6s exposure to oxygen plasma. The pores with characteristic dimensions ~ 1nm are clearly seen. (C) Raman spectra of graphene sample used for STEM imaging in (A,B) which shows I_D/I_G~1.

Table 1. Filtration of KCl solution (6 mM) through graphene membranes.

Sample	Feed solution conductivity	Water collected after 24 h	Permeate conductivity
SiN pore	950 μS/cm	7.2 mL	675 μS/cm
Graphene/SiN Pore	950 μS/cm	0 mL	-
Porous Graphene/SiN Pore (I_D/I_G = 0.6)	950 μS/cm	5.0 mL	<11 μS/cm

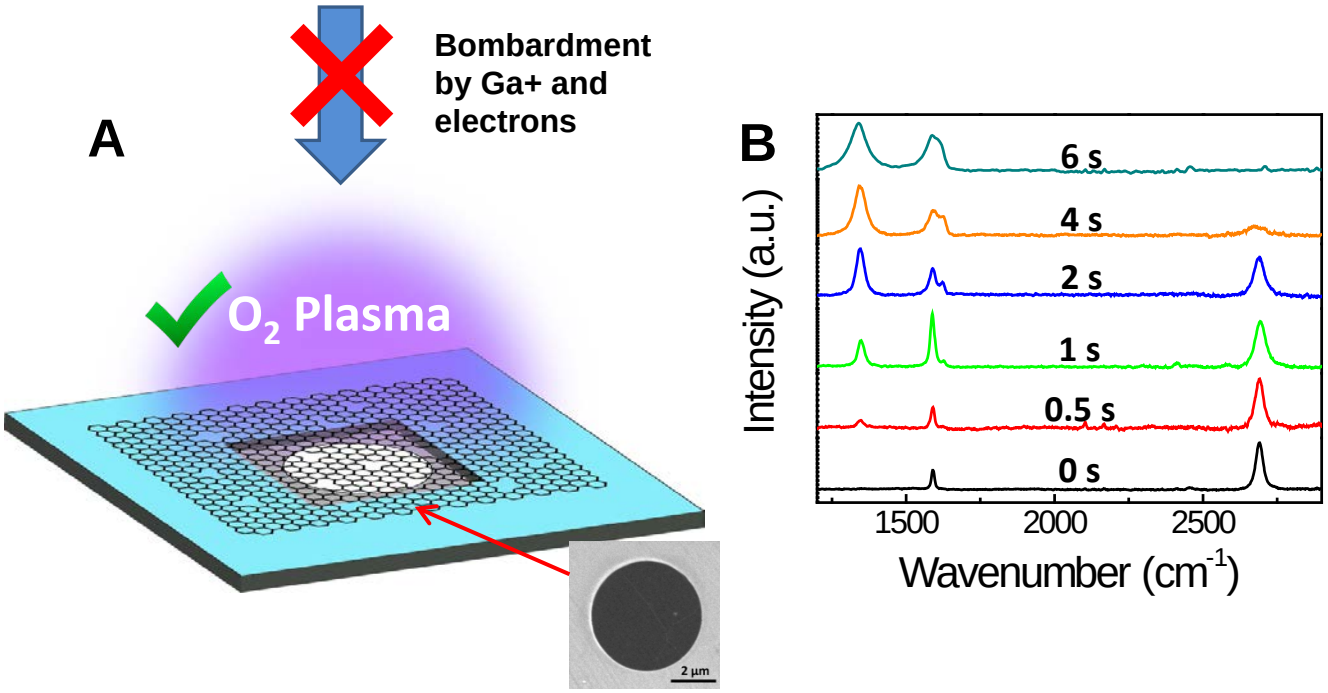
A
Bombardment by Ga+ and electrons
O2 Plasma
2 µm
B
6 s
4 s
2 s
1 s
0.5 s
0 s
Intensity (a.u.)
1500
2000
2500
Wavenumber (cm-1)

A

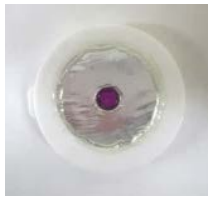

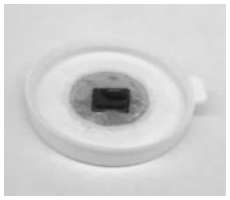

Graphene/Si wafer glued using epoxy and aluminum tape onto a container's lid

Si wafer with hole

Container lid glued onto container containing water using epoxy

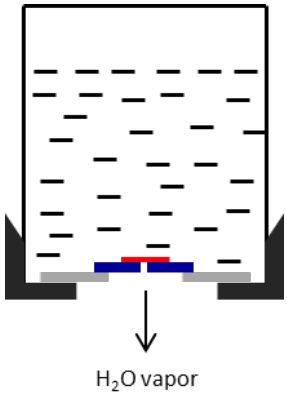

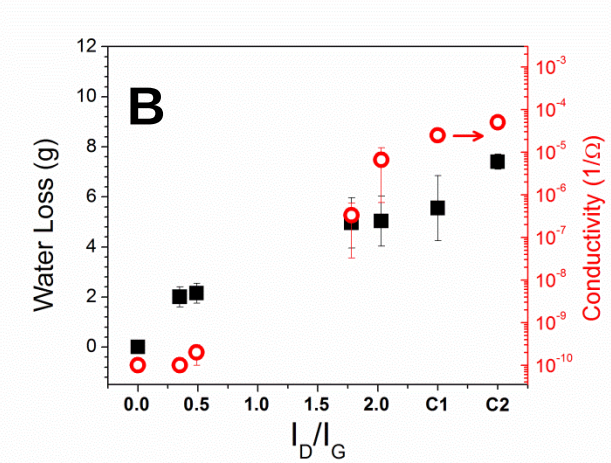

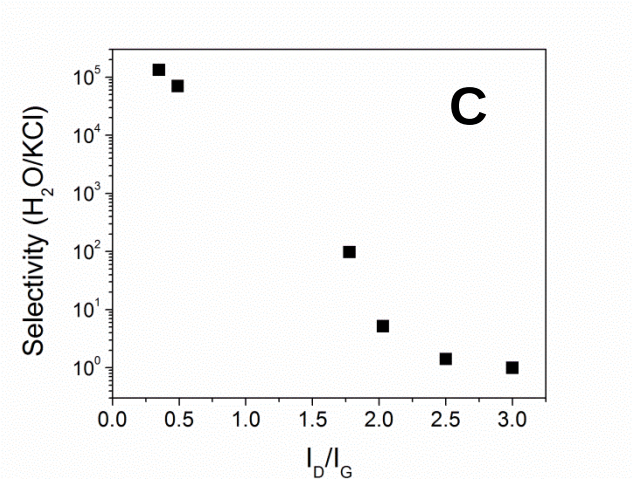

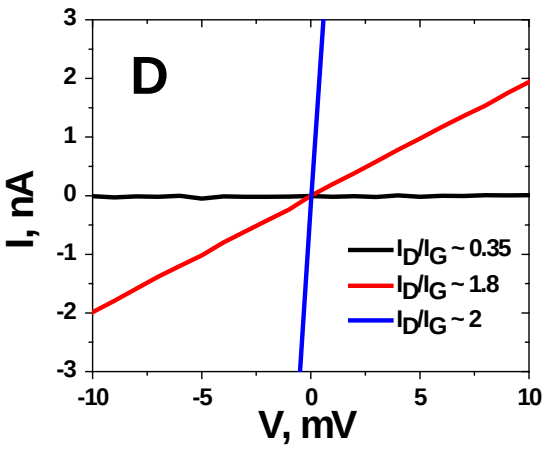

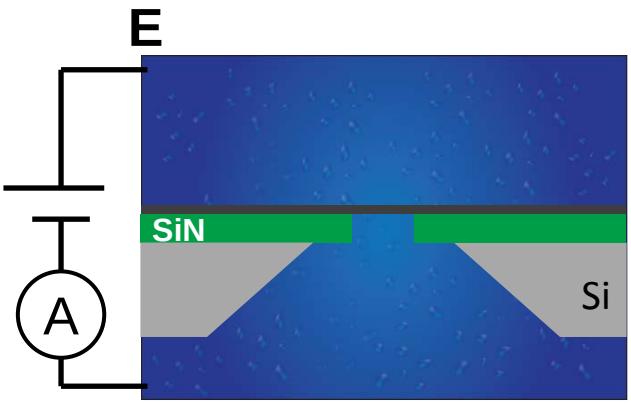

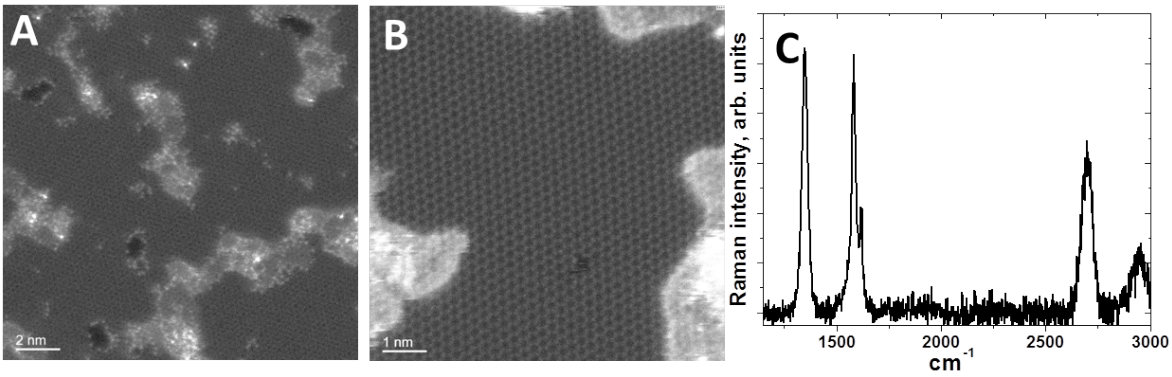
A
2 nm
B
1 nm
C
Raman intensity, arb. units
1500
2000
2500
3000
cm-1

Water Desalination Using Nanoporous Single-Layer Graphene with Tunable Pore Size

Sumedh P. Surwade,[1] Sergei N. Smirnov,[2] Ivan Vlassiouk,[3*] Raymond R. Unocic,[4] Sheng Dai,[1,5]* Shannon M. Mahurin[1]*

1. Estimation of defect density from Raman spectra

For defect density estimation, ratio I_G/I_D obtained from the Raman spectra is usually used. This ratio, however, is expected to depend not only on the defect density, but also on the types of defects, their size and arrangement against each other. Two empirical equations (Eq. S1 and S2), provide rough estimations for the defect density derived from I_G/I_D ratio when the defect density is not too high:[1,2]

$$L_a(nm) = \frac{560}{E_l^4}\frac{I_G}{I_D} \qquad \text{(S1)}$$

$$L_a(nm) = \left(-12.6 + \frac{40.9}{E_l}\right)\frac{I_G}{I_D} \qquad \text{(S2)}$$

where E_l is the excitation energy in eV, I_G and I_D are the intensities of G and D bands. respectively. The $L_a \sim I_G/I_D$ dependence should be valid for L_a down to 2 nm.[3] For L_a less than 2 nm L_a is proportional to $(I_G/I_D)^{-1/2}$.

In this work we used two excitation wavelengths for Raman spectra, 514nm (2.41eV) for oxygen plasma treatment and 633 nm (1.96eV) for bombardment by Ga^+ and electrons. A Renishaw 1000 Raman spectrometer with a Leica microscope were used to collect Raman data.

Sample used for STEM imaging (Fig.3 of the main text), has $I_G/I_D \sim 1$, which corresponds to L_a ~16 nm from Eq. S1 or $L_a \sim$ 5 nm from Eq. S2. Estimated from STEM images value of L_a lies in between, $L_a \sim$ 10nm (see Fig. S1).

Scanning transmission electron microscopy (STEM). Aberration-corrected STEM imaging was performed using a Nion UltraSTEM that is equipped with a cold-field emission gun as the electron source and capable of aberration correction of third and fifth order aberrations.[4] The STEM was operated at 60 kV, which is below the knock-on damage of graphene. Medium angle annular dark field (MAADF) STEM images were acquired with a convergence semi-angle of 30 mrad and a 54-200 mrad collection semi-angle. Prior to STEM imaging, the graphene specimens were baked for 8 hrs under vacuum at 160ºC in order to remove surface contamination. All of the STEM images presented here are raw and unprocessed.

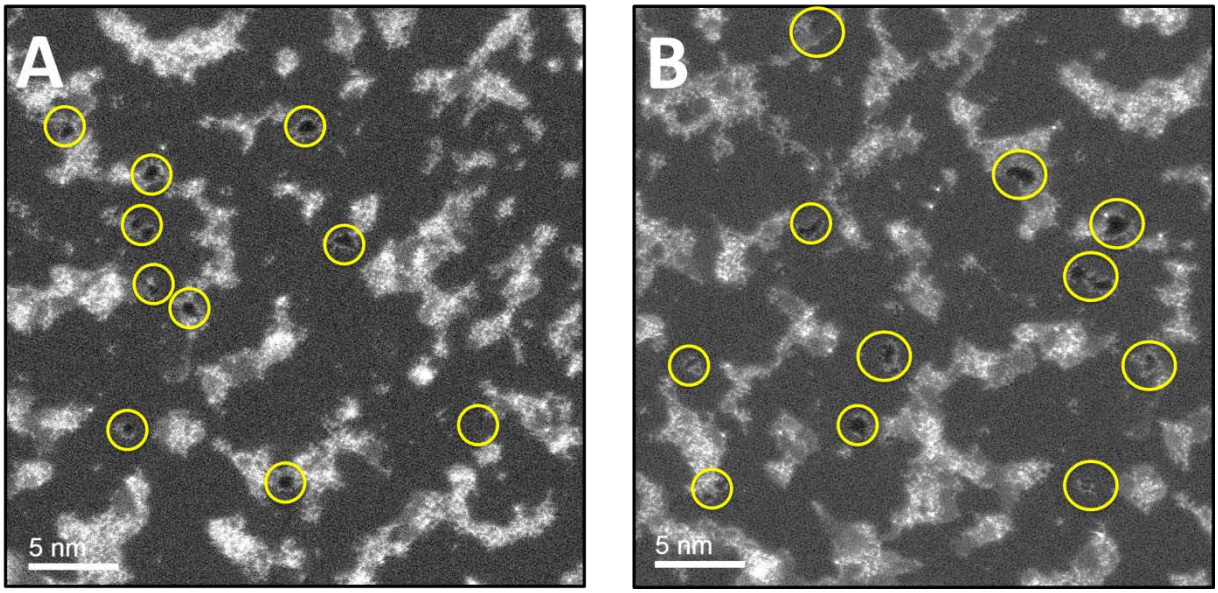

Figure S1. Large area, single layer graphene STEM image. The same sample as shown in Fig. 3 of the main text. Pore density is estimated to be 1 pore per 100 nm^2, which roughly translates to L_a~10nm for point defects.

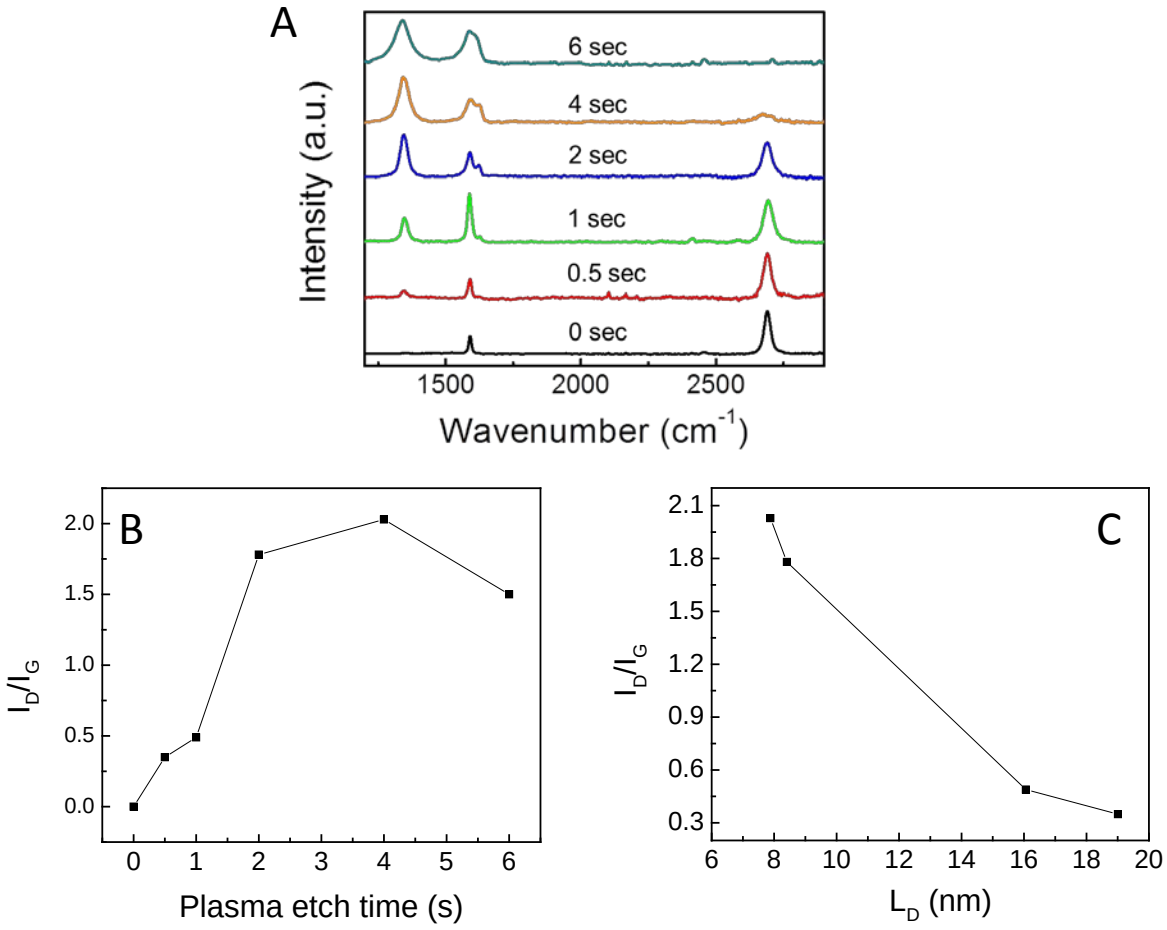

Figure S2. (A) Raman spectra of suspended graphene on exposure to plasma etch for different times. (B) Plot of plasma etch time vs I_D/I_G. (C) Plot of distance between defects L_D vs. I_D/I_G. As the plasma etch time increased, the I_D/I_G ratio increased due to the introduction of additional defects at longer exposure times.

2. Fabrication of graphene membranes

After synthesis, the graphene was transferred to the SiN microchip device with a 5 μm diameter hole. Each microchip was visually examined using SEM in order to ensure that there were no ruptures or tears in the graphene. Fig. S3 shows the SiN microchip devices that were used to collect the Raman spectra in Fig. 1B (and Fig. S3). The images of the two controls (C1 and C2) show clear ruptures while the remaining devices are intact with no visual holes. After passing this quality control step, the microchip devices were used for both water and ion transport measurements.

I_D/I_G	SEM image
0	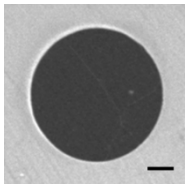
0.348	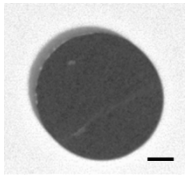
0.489	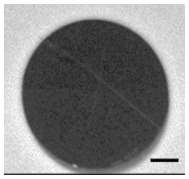
1.78	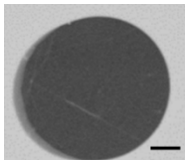
2.02	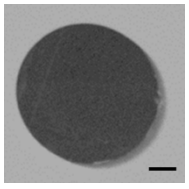
C1	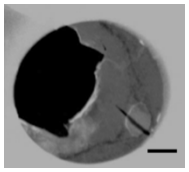

C2	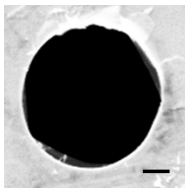

Figure S3. SEM images of samples of different defect density used in Fig. 2B (main manuscript). For each image, the scale bar is 1 μm.

3. Measurements of the ionic current through nanopores.

Ionic current was measured in the experimental setup (Fig. S2A) similar to that reported earlier.[5] In brief, 300nm thick SiN membrane with graphene covering 5μm diameter hole drilled by FIB was mounted in a custom made electrochemical cell with two Ag/AgCl wire electrodes on both sides of the membrane. Ionic current was measured by Keithley 6487 picoammeter interfaced by Matlab. The cell has two quartz windows allowing observation of the membrane surface by optical microscope. Membrane inspection under optical microscope is crucial for confirmation of complete wetting by electrolyte and absence of bubbles.

Fig. S4B shows an I-V curve for 5 μm hole without graphene (squares) and the current determined by Hall resistance and described by Eq. S3[6]

$$I \approx \frac{2aV}{\rho} \qquad \text{(S3)}$$

where a is the pore radius, V is the applied voltage and ρ is the solution conductivity. Our experimental setup allows ionic current measurements down to ~10 pA, which translates to 10 GΩ resistance limit at maximum applied voltages used in this work - 0.1V (Fig. S4C). Higher voltages applied across atomically thin graphene membranes resulted in peculiar membrane behavior which will be the topic of separate publication.

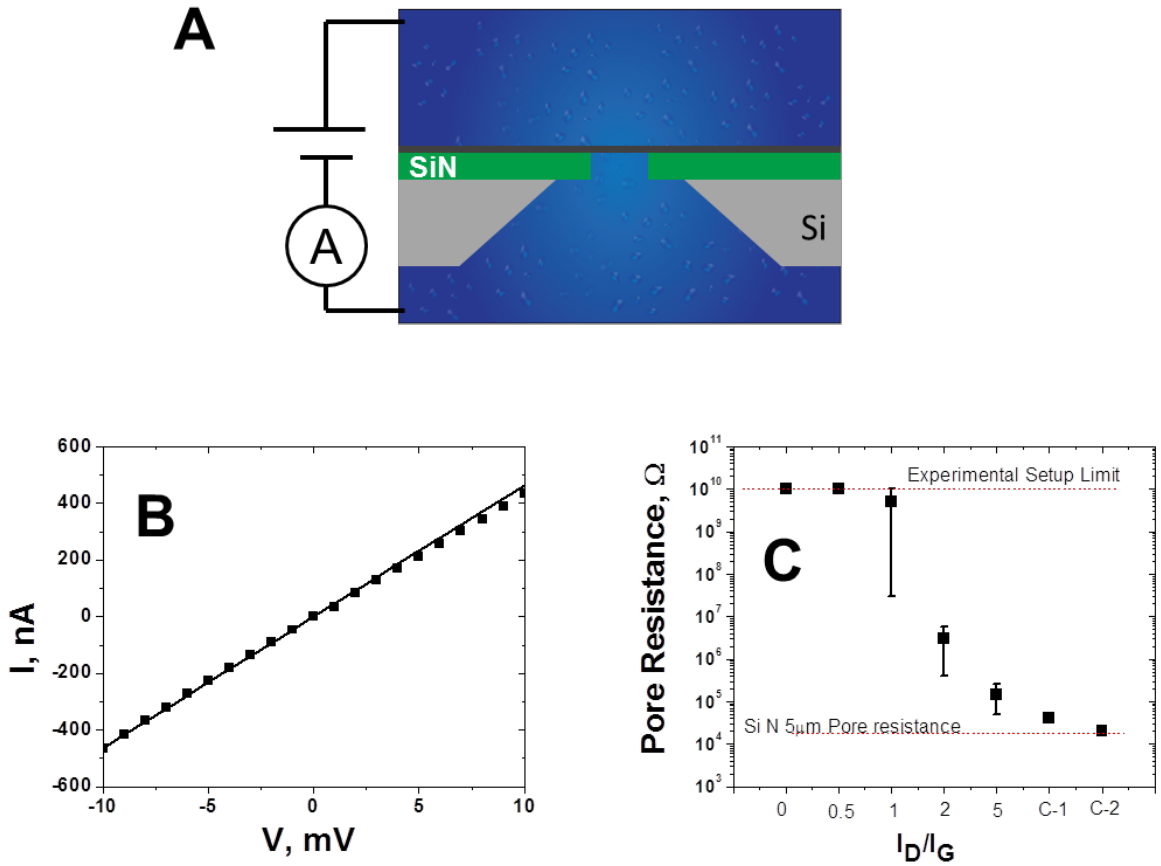

Figure S4. *Measurement of ionic current across graphene membrane.* (A) Scheme of experimental electrochemical cell. (B) Ionic current through 5μm hole in 300 nm thick SiN membrane using 1M KCl solution (squares) and the current limited by Hall resistance described by Eq. S3 (line). (C) Resistance of graphene membranes vs. I_D/I_G. C-1 is a control sample with partially raptured graphene membrane, whereas C-2 is the sample without graphene. I-V curve for similar to C-2 sample is shown on Fig. S2B.

4. Measurement of water transport.

Water transport measurements were performed by attaching the SiN microchip device onto the lid of container with a hole punched in it. After allowing the epoxy to cure, the lid was placed on the container partially filled with DI water (or KCl solution) and sealed. For pure DI water transport measurements, the container was then inverted so the water was in contact with the graphene and the entire assembly was placed in an oven maintained at 40 °C. The mass of the container was then measured periodically to determine the mass loss and water transport through the membrane. Blank SiN microchips with no hole were measured to ensure that no water was lost through the epoxy seals that might skew the transport results. For KCl solutions, a second container was added below the solution-filled container to collect transported water. The

conductivity of the initial solution was measured before the transport measurements and the collected water was carefully removed from the lower container and conductivity measured.

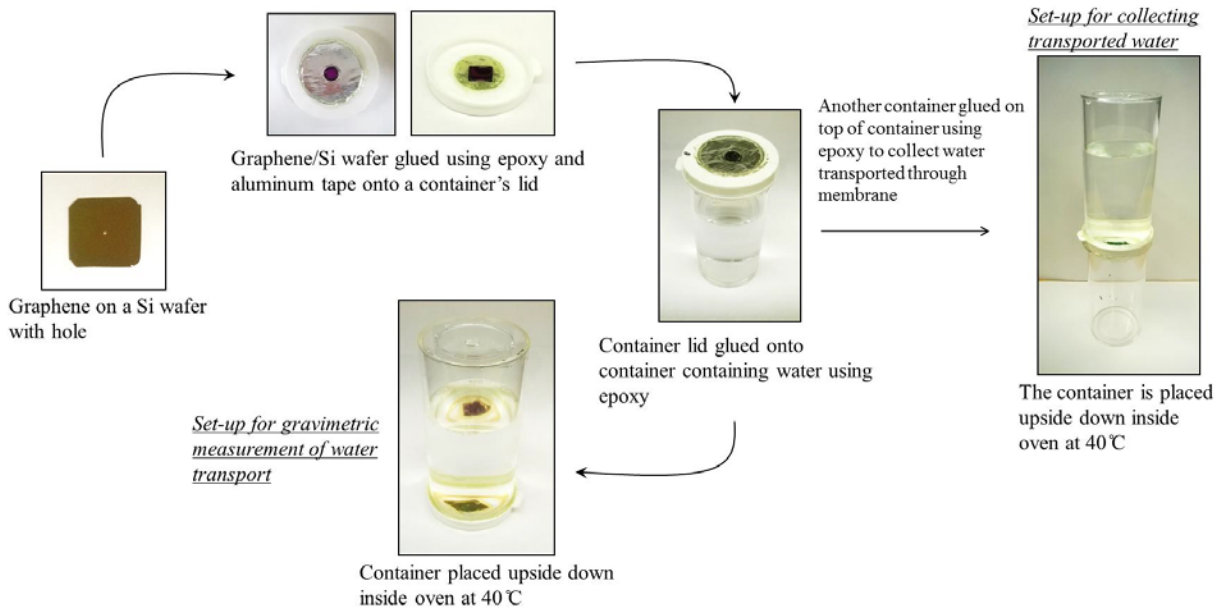

Figure S5. Schematics and images showing the experimental set-up.

5. Bombardment by electrons and Ga ions.

For comparison to the plasma etched samples, we also prepared porous graphene using electron and ion bombardment. Single layer graphene was transferred onto a silicon nitride TEM grid with 2.5 μm holes. Bombardment by electrons was done using Zeiss Merlin SEM by scanning the area for desired period of time, probe current and accelerating voltage. Irradiation by ions was done using dual beam FEI instrument by scanning the area for desired period of time. Accelerating voltage of 30kV and 1-10pA current beam was used. Bombardment by electrons and ions did not result in creating nanopore large enough for water molecules despite the broad range of dosage (up to 3100 electrons/nm^2 and 4ions/nm^2) corresponding to the density of defects up to 1/nm^2.

1 Cancado, L. G. *et al.* General equation for the determination of the crystallite size l-a of nanographite by raman spectroscopy. *Appl. Phys. Lett.* **88**, 163106 (2006).

2 Matthews, M. J., Pimenta, M. A., Dresselhaus, G., Dresselhaus, M. S. & Endo, M. Origin of dispersive effects of the raman d band in carbon materials. *Phys. Rev. B* **59**, R6585-R6588 (1999).
3 Ferrari, A. C. Raman spectroscopy of graphene and graphite: Disorder, electron-phonon coupling, doping and nonadiabatic effects. *Solid State Commun.* **143**, 47-57 (2007).
4 Krivanek, O. L. *et al.* An electron microscope for the aberration-corrected era. *Ultramicroscopy* **108**, 179-195 (2008).
5 Smirnov, S. N., Vlassiouk, I. V. & Lavrik, N. V. Voltage-gated hydrophobic nanopores. *ACS Nano* **5**, 7453-7461 (2011).
6 Vlassiouk, I., Smirnov, S. & Siwy, Z. Ionic selectivity of single nanochannels. *Nano. Lett.* **8**, 1978-1985 (2008).